Quadric Arrangement in Classifying Rigid Motions of a 3D Digital Image

Kacper Pluta[1,2], Guillaume Moroz[3], Yukiko Kenmochi[1], and Pascal Romon[2]

[1] Université Paris-Est, LIGM, CNRS, ESIEE Paris, France
kacper.pluta@univ-paris-est.fr
yukiko.kenmochi@esiee.fr
[2] Université Paris-Est, LAMA, UPEM, France
pascal.romon@u-pem.fr
[3] INRIA Nancy-Grand-Est, Project Vegas, France
guillaume.moroz@inria.fr

Abstract. Rigid motions are fundamental operations in image processing. While bijective and isometric in $\mathbb{R}^3$, they lose these properties when digitized in $\mathbb{Z}^3$. To understand how the digitization of 3D rigid motions affects the topology and geometry of a chosen image patch, we classify the rigid motions according to their effect on the image patch. This classification can be described by an arrangement of hypersurfaces in the parameter space of 3D rigid motions of dimension six. However, its high dimensionality and the existence of degenerate cases make a direct application of classical techniques, such as cylindrical algebraic decomposition or critical point method, difficult. We show that this problem can be first reduced to computing sample points in an arrangement of quadrics in the 3D parameter space of rotations. Then we recover information about remaining three parameters of translation. We implemented an ad-hoc variant of state-of-the-art algorithms and applied it to an image patch of cardinality 7. This leads to an arrangement of 81 quadrics and we recovered the classification in less than one hour on a machine equipped with 40 cores.

1 Introduction

Rigid motions (*i.e.*, rotations, translations and their compositions) defined on $\mathbb{Z}^3$ are simple yet crucial operations in many image applications (*e.g.*, image registration [33] and motion tracking [32]). However, it is also known that such operations cause geometric and topological defects [18,19,22]. As such alterations happen locally, due to digitization, discrete motion maps have been studied for small image patches, in order to understand such defects at local scale [20,21,23].

For such a local analysis, one wishes to generate all possible images of an image patch under digitized rigid motions. In digital geometry and combinatorics, some complexity analysis of such a problem has been made for some geometric transformations. The complexities are related to the size of a given image patch in general: $O(n^3)$ for 2D rotations [2]; $O(n^9)$ for 2D rigid motions [17] and $O(n^{18})$ for 2D affine transformations [10], where n stands for a diameter of a subset of an image patch. Later, in this article we show that the theoretical complexity of such a problem for 3D rigid motions is $O(n^{24})$.

However, there are few algorithms available for generating all the transformed images from a given image patch. Algorithms known to us are: 2D rotations [21]; 3D rotations around a given rational axis [30, 31]; 2D rigid motions [17, 23] and 2D affine transformations [10]. However, none of them can be applied to 3D rigid motions.

In this article, we reformulate this classification problem on a finite digital image as an arrangement of quadrics, containing many degenerate cases. We then solve the problem by computing all the 3D open cells in this arrangement. The original problem involves a naive decomposition of the six dimensional parameter space of 3D rigid motions, and can be formulated as an arrangement of hypersurfaces given by polynomials of degree two with integer coefficients. Our goal is to compute for each full–dimensional open cell at least one representative point, so-called *sample point*. The state-of-the-art techniques such as cylindrical algebraic decomposition or critical point method [3] are burdened by double exponential [5] and exponential [26] complexity respectively, with respect to the number of variables. Therefore, their direct application to the problem of decomposition of the six dimensional parameter space of 3D digitized rigid motions are practically inefficient. Indeed, high dimensionality and existence of cases such as asymptotic critical values [13]—*e.g.*, a plane orthogonal to a coordinate axis is tangent to a hypersurface in a point at infinity—make a computation of such an arrangement difficult.

In this article, we propose an ad-hoc method as follows. We first show that the problem can be simplified by uncoupling the six parameters of 3D rigid motions to end up with two systems in three variables, and start by studying an arrangement of quadrics in $\mathbb{R}^3$. These two systems correspond to the rotational and translational parameters of rigid motions, respectively. In order to detect all topological changes along one non-generic, chosen direction by sweeping a plane, we compute all critical points including asymptotic critical values in this arrangement of quadrics. Moreover, we compute at least one sample point for each open full dimensional cell in the arrangement – sample points of full dimensional components provide information to generate different images of an image patch under digitized rigid motions. Our strategy is similar to the one proposed by Mourrain *et al.* [15] where the main differences are: we do not use generic directions; we handle asymptotic cases and give new criteria to compute critical values in polynomials of degree two; we compute and store at least one sample point for each full dimensional open cell where Mourrain *et al.* [15] compute full adjacency information for all cells in an arrangement; moreover, we precompute all critical values *a priori* while in the former approach only one type of critical values needs to be computed before the main algorithm. Those sample points are then used to decompose the other three dimensional parameter space. Finally, our implementation is provided together with a numerical experiment for a small image patch.

2 Classifying Rigid Motions of a 3D Digital Image

2.1 Rigid Motions on the 3D Cartesian Grid

Rigid motions on $\mathbb{R}^3$ are bijective isometric maps defined as

$$\left|\begin{array}{l} \mathcal{U} : \mathbb{R}^3 \to \mathbb{R}^3 \\ \qquad \mathbf{x} \quad \mapsto \mathbf{R}\mathbf{x} + \mathbf{t} \end{array}\right. \tag{1}$$

where $\mathbf{t} = (t_1, t_2, t_3) \in \mathbb{R}^3$ is a translation vector and $\mathbf{R}$ is a rotation matrix. Let $\mathbf{A}$ be a skew-symmetric matrix

$$\mathbf{A} = \begin{bmatrix} 0 & c & -b \\ -c & 0 & a \\ b & -a & 0 \end{bmatrix}$$

where $a, b, c \in \mathbb{R}$ and $\mathbf{I}$ be the 3×3 identity matrix. Then almost any rotation matrix $\mathbf{R}$ can be obtained by the Cayley transform [4]:

$$\begin{aligned} \mathbf{R} &= (\mathbf{I} - \mathbf{A})(\mathbf{I} + \mathbf{A})^{-1} \\ &= \frac{1}{1 + a^2 + b^2 + c^2} \begin{bmatrix} 1 + a^2 - b^2 - c^2 & 2(ab - c) & 2(b + ac) \\ 2(ab + c) & 1 - a^2 + b^2 - c^2 & 2(bc - a) \\ 2(ac - b) & 2(a + bc) & 1 - a^2 - b^2 + c^2 \end{bmatrix}. \end{aligned} \tag{2}$$

Indeed, rotations by π around any axis can only be obtained by the Cayley transform as a limit: angles of rotation converge to π when a, b, c tend to infinity [29]. In practice, this constraint is negligible and does not affect generality of our study (see the following section which discusses the evolution of an image patch under 3D digitized rigid motions). Using this formula, a rigid motion is parametrized by the six real parameters (a, b, c, t_1, t_2, t_3).

According to Equation (1), we generally have $\mathcal{U}(\mathbb{Z}^3) \nsubseteq \mathbb{Z}^3$. As a consequence, in order to define digitized rigid motions as maps from $\mathbb{Z}^3$ to $\mathbb{Z}^3$, we combine, as usual, the results of the rotation with a digitization operator

$$\begin{vmatrix} \mathcal{D} : \mathbb{R}^3 & \to \mathbb{Z}^3 \\ (x_1, x_2, x_3) & \mapsto \left(\left\lfloor x_1 + \frac{1}{2} \right\rfloor, \left\lfloor x_2 + \frac{1}{2} \right\rfloor, \left\lfloor x_3 + \frac{1}{2} \right\rfloor \right) \end{vmatrix}$$

where $\lfloor s \rfloor$ denotes the largest integer not greater than s. The digitized rigid motion is thus defined by $U = \mathcal{D} \circ \mathcal{U}_{|\mathbb{Z}^3}$. Due to the behavior of $\mathcal{D}$ that maps $\mathbb{R}^3$ onto $\mathbb{Z}^3$, digitized rigid motions are, most of the time, non–bijective. However, some are, and an algorithmic approach to these digitized rotations is given in [24].

2.2 Image Patch and its Alterations Under Digitized 3D Rigid Motions

Let us consider a finite set $\mathcal{N} \subset \mathbb{Z}^3$, called an *image patch* whose center $\mathbf{c}$ and radius r of $\mathcal{N}$ are given by $\mathbf{c} = \frac{1}{|\mathcal{N}|} \sum_{\mathbf{v} \in \mathcal{N}} \mathbf{v}$ and $r = \max_{\mathbf{v} \in \mathcal{N}} \|\mathbf{v} - \mathbf{c}\|$, respectively. Note that, in this article, we consider $\mathbf{c}$ as the origin, for simplicity. Next, we express the evolution of such an image patch $\mathcal{N}$ under digitized rigid motions U.

The digitized rigid motions $U = \mathcal{D} \circ \mathcal{U}$ are piecewise constant, and thus non-continuous, which is a consequence of the nature of the digitization operator $\mathcal{D}$. In particular, the image $\mathcal{U}(\mathbf{v})$ of a given point $\mathbf{v}$ may remain constant as the parameters of $\mathcal{U}$ vary, and then suddenly jump from one point of $\mathbb{Z}^3$ to another. In other words, an image patch $\mathcal{N}$ evolves non-continuously, under digitized rigid motions, in accordance with the parameters of $\mathcal{U}$ that underlies U (see Figure 1). Hereafter, without loss of generality we assume that $\mathcal{U}(\mathbf{c})$ stays in the digitization cell of $\mathbf{c}$, namely $U(\mathbf{c}) = \mathbf{c}$,

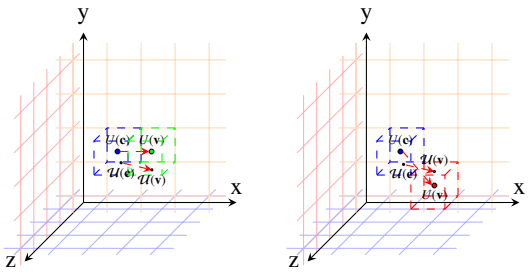

(a) (b)

Fig. 1. An example of discontinuity of U. In (a) and (b) the image $\mathcal{U}(\mathbf{c})$ remains within the same unit cube—digitization cell—centered around the origin depicted in blue; thus the image $U(\mathbf{c})$ is the same for the two digitized motions U associated to the continuous motions $\mathcal{U}$ that slightly differ with respect to the parameters. However, the point $\mathbf{v} = \mathbf{c} + (1, 0, 0)^t$, has distinct images $U(\mathbf{v})$ in (a) and (b); in (a), the digitization operator $\mathcal{D}$ sends $\mathcal{U}(\mathbf{v})$ onto the green integer point, while in (b), it sends it onto the red one

since translation by an integer vector would not change the geometry of $\mathcal{N}$. Under this assumption we have that $\mathbf{t} \in \left(-\frac{1}{2}, \frac{1}{2}\right]^3$. Moreover, thanks to symmetry (reflections and rotations) we consider only non-negative a, b, c.

Studying the non-continuous evolution of an image patch $\mathcal{N}$ is equivalent to study the discontinuities of $U(\mathbf{v})$ for every $\mathbf{v} \in \mathcal{N} \setminus \{\mathbf{c}\}$, which occur when $\mathcal{U}(\mathbf{v})$ is on the *half-grid* plane, namely a boundary of a digitization cell. This is formulated by

$$\mathbf{R}_i \mathbf{v} + t_i = k_i - \frac{1}{2} \tag{3}$$

where $k_i \in H(\mathcal{N}) = \mathbb{Z} \cap [-r', r']$, $\mathbf{R}_i$ is the i-th row of the rotation matrix for $i \in \{1, 2, 3\}$ and r' is the longest radius of $\mathcal{U}(\mathcal{N})$ for all $\mathcal{U}$, so that $r' = r + \sqrt{3}$.

3 Arrangement of Quadrics

3.1 The Problem as an Arrangement of Hypersurfaces

For any image patch $\mathcal{N}$, the parameter space

$$\Omega = \left\{ (a, b, c, t_1, t_2, t_3) \in \mathbb{R}^6 \mid a, b, c \geq 0, -\frac{1}{2} < t_i < \frac{1}{2} \text{ for } i = 1, 2, 3 \right\}$$

is partitioned by a set of hypersurfaces given by Equations (3) into a finite number of connected subsets, namely, 6D open cells whose points induces different rigid motions $\mathcal{U}_{|\mathcal{N}}$ but identical digitized rigid motions $U_{|\mathcal{N}} = \mathcal{D} \circ \mathcal{U}_{|\mathcal{N}}$. For a given image patch $\mathcal{N}$ of radius r, hypersurfaces (3) in Ω are given by the possible combinations of integer 4–tuples (v_1, v_2, v_3, k_i) for $i = 1, 2, 3$ where $\mathbf{v} = (v_1, v_2, v_3) \in \mathcal{N} \setminus \{\mathbf{c}\}$ and $k_i \in H(\mathcal{N})$. Since $|\mathcal{N}| - 1$ is in $O(r^3)$ and $|H(\mathcal{N})|$ is in $O(r)$, the number of considerable hypersurfaces is in $O(r^4)$, and thus in accordance with [8, Theorem 21.1.4] the overall complexity of the arrangement is theoretically bounded by $O(r^{24})$.

Our goal is to compute for each 6D open cell in Ω at least one representative point, a so-called *sample point*. As the direct application of the cylindrical algebraic

decomposition or critical points method to this problem is practically inefficient – due to the high dimensionality and existence of degenerate cases that make computation of the arrangement difficult. Therefore, in the following discussion we develop an indirect but still exact strategy.

3.2 Uncoupling the Parameters

The first idea of our strategy consists in uncoupling the parameters in the six dimensional parameter space Ω. Namely, we show that by considering the differences between the hypersurfaces given in Equation (3) for different $\mathbf{v} \in \mathcal{N}$ and $\mathbf{k} \in H(\mathcal{N})^3$, we can reduce the problem to the study of an arrangement of surfaces in the (a, b, c)–space, and then lift the solution to the six dimensional space.

Let us consider a rigid motion defined by $\mathbf{R}$ and $\mathbf{t}$. The condition for having $U(\mathbf{v}) = \mathbf{k} = (k_1, k_2, k_3) \in \mathbb{Z}^3$ where $\mathbf{v} \in \mathcal{N}$ is

$$k_i - \frac{1}{2} < \mathbf{R}_i\mathbf{v} + t_i < k_i + \frac{1}{2}$$

for $i = 1, 2, 3$. Equivalently,

$$k_i - \frac{1}{2} - \mathbf{R}_i\mathbf{v} < t_i < k_i + \frac{1}{2} - \mathbf{R}_i\mathbf{v}. \tag{4}$$

Let us call a *configuration* a list of couples $(\mathbf{v}, \mathbf{k})$, which describe how the image patch $\mathcal{N}$ is transformed. This configuration can be described as a function

$$\left| \begin{array}{ll} F : \mathcal{N} & \to H(\mathcal{N})^3 \\ \quad \mathbf{v} = (v_1, v_2, v_3) & \mapsto \mathbf{k} = (k_1, k_2, k_3). \end{array} \right.$$

We want to ascertain whether a given configuration F arises from some digitized rigid motion U, *i.e.*, corresponds to some parameters a, b, c, t_1, t_2, t_3. Then the inequalities (4) state precisely the necessary and sufficient conditions for the existence of the translation part $\mathbf{t}$ of such a rigid motion, assuming that a, b, c are already known. Let us now remark that all these inequalities can be summed up in *three* inequalities indexed by i:

$$\max_{\mathbf{v}\in\mathcal{N}} \left(F(\mathbf{v})_i - \frac{1}{2} - \mathbf{R}_i\mathbf{v} \right) < \min_{\mathbf{v}\in\mathcal{N}} \left(F(\mathbf{v})_i + \frac{1}{2} - \mathbf{R}_i\mathbf{v} \right). \tag{5}$$

or, equivalently to the following list of inequalities

$$\forall \mathbf{v}, \mathbf{v}' \in \mathcal{N}, \quad F(\mathbf{v}')_i - \frac{1}{2} - \mathbf{R}_i\mathbf{v}' < F(\mathbf{v})_i + \frac{1}{2} - \mathbf{R}_i\mathbf{v}. \tag{6}$$

The key observation is that we have eliminated the variables t_1, t_2, t_3 and have reduced to a subsystem of inequalities in a, b, c. Moreover, due to the rational expression in the Cayley transform (2), we may use the following polynomials of degree 2:

$$q_i[\mathbf{v}, k_i](a, b, c) = (1 + a^2 + b^2 + c^2)(2k_i - 1 - 2\mathbf{R}_i\mathbf{v}), \tag{7}$$

for $i = 1, 2, 3$, namely

$$q_1[\mathbf{v}, k_1](a, b, c) = -2(1 + a^2 - b^2 - c^2)v_1 - 4(ab - c)v_2 - 4(b + ac)v_3 + 2k_1 - 1,$$

$$q_2[\mathbf{v}, k_2](a, b, c) = -4(ab + c)v_1 - 2(1 - a^2 + b^2 - c^2)v_2 - 4(bc - a)v_3 + 2k_2 - 1,$$

$$q_3[\mathbf{v}, k_3](a, b, c) = -4(ac - b)v_1 - 4(a + bc)v_2 - 2(1 - a^2 - b^2 + c^2)v_3 + 2k_3 - 1.$$

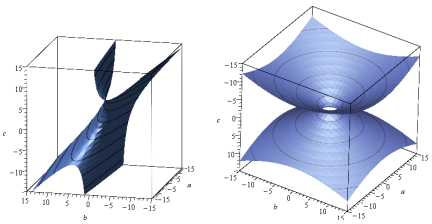

(a) (b)

Fig. 2. Examples of the zero sets of two quadratic polynomials of $\mathcal{Q}$

Inequality (6) can be rewritten as the quadratic polynomial inequalities

$$\forall \mathbf{v}, \mathbf{v}' \in \mathcal{N}, \quad Q_i[\mathbf{v}, \mathbf{v}', F(\mathbf{v})_i, F(\mathbf{v}')_i](a, b, c) > 0,$$

where

$$Q_i[\mathbf{v}, \mathbf{v}', k_i, k_i'](a, b, c) = q_i[\mathbf{v}, k_i](a, b, c) + 2(1 + a^2 + b^2 + c^2) - q_i[\mathbf{v}', k_i'](a, b, c), \quad (8)$$

for $i = 1, 2, 3$. The set of quadratic polynomials for our problem is then given by $\mathcal{Q} = \{Q_i[\mathbf{v}, \mathbf{v}', k_i, k_i'](a, b, c) \mid i = 1, 2, 3, \mathbf{v}, \mathbf{v}' \in \mathcal{N}, k_i, k_i' \in H(\mathcal{N})\}$. Figure 2 illustrates the zero sets of some quadratic polynomials in $\mathcal{Q}$.

4 Computing an Arrangement of Quadrics in 3D

In this section we discuss how to compute the arrangement of quadrics $Q(a, b, c) = 0$ for $Q \in \mathcal{Q}$ given by Equation (8). Our strategy is similar to one proposed by Mourrain *et al.* [15]. The main differences are that we do not store information about cells different from sample points of full dimensional connected components and we precompute and sort all event points—points which induce changes of topology in an arrangement of quadrics—*a priori*. Moreover, we consider cases such as asymptotic critical values. In short, our method is as follows: Step 1: detect and sort all the events in which topology of an arrangement changes; Step 2: sweep by a plane the set of quadrics along a chosen direction. The sweeping plane stops between two event points and we project quadrics related to them onto the sweeping plane. This reduces to the problem of 2D arrangement of conics for each of such points. After this procedure, for each sample point we recover the translation part of the parameter space of digitized 3D rigid motions. The description of this last part will be given in the next section. Notice that proposed approach could be also applied to solve a similar problem in 2D, *i.e.*, generation of the different images of a 2D image patch under 2D digitized rigid motions – a solution to this problem was already proposed by Ngo *et al.* [17].

4.1 Bifurcation and Critical Values

In [15], the authors show how to describe an arrangement of quadric by sweeping a plane along a generic direction. Using the theory of *generalized critical values* [12, 13, 25] we will show how to compute a point per open connected component of an arrangement of quadric using a projection along a non-generic direction.

In the following, we consider an arrangement of smooth quadrics $S_i \subset \mathbb{R}^3$ defined by $Q_i(a,b,c) = 0$ for all $Q_i \in \mathcal{Q}$. Note that, if quadric S_i has isolated singularities then without loss of generality one can remove them and work with remaining smooth parts of S_i. We denote by $\mathcal{A}$ the set of maximally connected components of $\mathbb{R}^3 \setminus \bigcup_i S_i$.

Let $\mathcal{C}$ be an open cell of $\mathcal{A}$. We can associate to $\mathcal{C}$ the extremal values $\mathcal{C}_{\text{inf}} = \inf\{a \mid (a,b,c) \in \mathcal{C}\}$ and $\mathcal{C}_{\text{sup}} = \sup\{a \mid (a,b,c) \in \mathcal{C}\}$. We will show in this section that these values are included in a *bifurcation set* (see Definition 1).

In the following, for $i, j, k \in \mathbb{Z}$, we denote by S_i the surface defined by $Q_i(a,b,c) = 0$, by C_{ij} the curve defined by $Q_i = Q_j = 0$ and by P_{ijk} the points defined by $Q_i = Q_j = Q_k = 0$. Furthermore, we assume that S_i are smooth surfaces of dimension two, the C_{ij} are smooth curves of dimension one and $\rho(P_{ijk})$ are finite sets of values.

The projection map on the first coordinate a is denoted by ρ, and its restriction to a submanifold $\mathcal{M} \subset \mathbb{R}^3$ is denoted by $\rho_{|\mathcal{M}}$. Moreover, for $a_0 \in \mathbb{R}$ we denote by $\mathcal{M}_{a_0}$ the set $\rho^{-1}_{|\mathcal{M}}(a_0)$. Similarly, for an open interval $]a_0, b_0[\subset \mathbb{R}$ we denote by $\mathcal{M}_{]a_0,b_0[}$ the set $\rho^{-1}_{|\mathcal{M}}(]a_0, b_0[)$.

We are interested in computing the set of values a above which the topology of the cells of $\mathcal{A}$ change. We will show in Lemma 2 that this set is included in the bifurcation set of the projections on the first axis restricted to different manifolds.

Definition 1. *Let $\mathcal{M}$ be a submanifold of $\mathbb{R}^3$. We call* bifurcation set *of $\rho_{|\mathcal{M}}$ the smallest set $B(\rho_{|\mathcal{M}}) \subset \mathbb{R}$ such that $\rho : \mathcal{M} \setminus \rho^{-1}(B(\rho_{|\mathcal{M}})) \to \mathbb{R} \setminus B(\rho_{|\mathcal{M}})$ is a locally trivial fibration.*

More specifically, for all $a_0 \in \mathbb{R} \setminus B(\rho_{|\mathcal{M}})$, there exists $\epsilon > 0$ and a homeomorphism

$$\psi :]a_0 - \epsilon, a_0 + \epsilon[\times \mathcal{M}_{a_0} \to \mathcal{M}_{]a_0-\epsilon,a_0+\epsilon[},$$

such that $\rho \circ \psi(x,p) = x$ for all $(x,p) \in]a_0 - \epsilon, a_0 + \epsilon[\times \mathcal{M}_{a_0}$.

In the following, we will consider the finite set $B \subset \mathbb{R}$ defined as the union of the bifurcation sets of $\rho_{|S_i}$ and $\rho_{|C_{ij}}$ and the projections of P_{ijk}. More precisely, we define:

$$B_i = B(\rho_{|S_i}) \cup \bigcup_{j \neq i} B(\rho_{|C_{ij}}) \cup \bigcup_{j \neq i, k \neq i, j \neq k} \rho(P_{ijk})$$

and $B = \bigcup_i B_i$.

Lemma 2. *Let $\mathcal{C}$ be a maximal open connected cell of $\mathbb{R}^3 \setminus \bigcup_i S_i$. Let β be the smallest value of B such that $\mathcal{C}_{\text{inf}} < \beta$ and let $a_0 \in]\mathcal{C}_{\text{inf}}, \beta[$. Finally, let $\partial\mathcal{C}_{a_0}$ be the boundary of $\mathcal{C}_{a_0}$ and $J_{\mathcal{C}}$ be its edges. More precisely, $J_{\mathcal{C}}$ is the set of indices i such that the intersection of S_i with $\partial\mathcal{C}_{a_0}$ has dimension one. Then $\mathcal{C}_{\text{inf}} \in B_i$ for all $i \in J_{\mathcal{C}}$.*

Proof. Let $i \in J_{\mathcal{C}}$ and let p be a point on $S_i \cap \partial\mathcal{C}_{a_0}$ that does not belong to any surface S_j for $j \neq i$. Let $\alpha \leq \mathcal{C}_{inf}$ be the maximal point of B_i less than a_0. Then $\rho_{|S_i}$ and $\rho_{|C_{ij}}$ are trivial fibrations above $]\alpha, \beta[$ and $\rho(P_{ijk}) \cap]\alpha, \beta[= \emptyset$ for $j \neq i$ and $k \neq i$ different integers. In particular, the points of the curves C_{ij} never cross above $]\alpha, \beta[$. More formally, there exists a continuous function $\phi :]\alpha, \beta[\to S_i$ such that $\phi(a_0) = p$ and $\rho \circ \phi(x) = x$ and $Q_j(\phi(x)) \neq 0$ for all $j \neq i$. Let T_ϵ be the tube defined by $T_\epsilon = \{(a,b,c) \in \mathbb{R}^3 \mid a \in [\mathcal{C}_{\text{inf}}, a_0] \text{ and } \|(a,b,c) - \phi(a)\| < \epsilon\}$. We now prove by contradiction that $\alpha = \mathcal{C}_{\text{inf}}$. If $\alpha < \mathcal{C}_{\text{inf}}$, then there exists a sufficiently small $\epsilon > 0$ such that the respective intersections of T_ϵ with $Q_i < 0$ and $Q_i > 0$ are connected and such

that T_ϵ does not intersect any S_j for $j \neq i$. Since $p \in T_\epsilon$, the intersection of T_ϵ with $\mathcal{C}$ is not empty. Moreover, $\mathcal{C}$ is a maximally connected component in the complement of the union of the S_j, such that one of the two connected component of $T_\epsilon \setminus S_i$ is included in $\mathcal{C}$. Thus, the tube T_ϵ intersects $\mathcal{C}_a$ for all $a \in [\mathcal{C}_{\text{inf}}, a_0]$. In particular $\mathcal{C}_{\mathcal{C}_{\text{inf}}}$ is not empty, which is a contradiction with the definition of $\mathcal{C}_{\text{inf}}$. In particular, $\mathcal{C}_{\text{inf}} = \alpha$, which allows us to conclude that $\mathcal{C}_{\text{inf}} \in B_i$. □

Figure 5 illustrates intervals such that the topology of $\mathcal{C}_a$, $a \in]\alpha, \beta[$ remains constant.

For each value $v_0 \in B$, we denote by $J_a \subset \mathbb{N}$ the set of indices i such that $v_0 \in B_i$. Moreover, for a set of indices J, we denote by $\mathcal{A}_J$ the set of maximally open connected components of $\mathbb{R}^3 \setminus \bigcup_{j \in J} S_j$.

Corollary 3. *Let $\mathcal{C}$ be a maximal open connected cell of $\mathbb{R}^3 \setminus \bigcup_i S_i$. Let $m > \mathcal{C}_{\text{inf}}$ be the smallest value of B greater than $\mathcal{C}_{\text{inf}}$. For all $a \in]\mathcal{C}_{\text{inf}}, m[$, there exists a cell $\mathcal{C}' \in \mathcal{A}_{J_{\mathcal{C}_{\text{inf}}}}$ such that $\mathcal{C}'_a \subset \mathcal{C}_a$.*

Proof. According to Lemma 2, $\mathcal{C}_{\text{inf}}$ is contained in all B_i such that S_i intersects the border of $\mathcal{C}_a$ with dimension one. In particular, one of the cells of $\mathcal{A}_{J_{\mathcal{C}_{\text{inf}}}} \cap \rho^{-1}(a)$ is included in $\mathcal{C}_a$. □

From a constructive point of view, the authors of [12] showed that the bifurcation set is included in the union of the critical and asymptotic critical values. More specifically, given a polynomial map $f : \mathcal{M} \to \mathbb{R}$, we have $B(f) \subset K(f) \cup K_\infty(f)$, where $K(f)$ are the critical values of f and K_∞ are its asymptotic critical values. In [15], the authors called the points of $K(\rho_{|S_i})$ events of type A, the points of $K(\rho_{|C_{ij}})$ events of type B and the points $\rho(P_{ijk})$ events of type C. We extended their classification for degenerate projections, and we say that the points of $K_\infty(\rho_{|S_i})$ are of type A_∞ and the points of $K_\infty(\rho_{|C_{ij}})$ are of type B_∞.

From a computational point of view, we recall in the next section how to compute the critical values of types A, B and C. For the types A_∞ and B_∞, we use the results from [12] and simplify them for the case of quadrics.

Finally as described in Subsection 4.4, our strategy will be to compute the generalized critical values a and for each value, we store also J_a the set of indices i such that either:

- $a \in K(\rho_{|C_i}) \cup K_\infty(\rho_{|C_i})$
- $a \in K(\rho_{|C_{ij}}) \cup K_\infty(\rho_{|C_{ij}})$ for $j \neq i$
- $a \in \rho(P_{ijk})$ for $j \neq i, k \neq i$ and $j \neq k$

This will allow us to reduce the number of quadrics to consider in the intermediate steps of our sweeping plane algorithm.

4.2 Detection of Critical Values

Type A. The first type corresponds to values $s \in K(\rho_{|S_i})$ above which topology of open connected components in $\mathcal{A}$ changes. Algebraically, such an event corresponds to a value of $s = a$—called a-critical value—for which there is a solution to the system $Q_i(s, b, c) = \partial_b Q_i(s, b, c) = \partial_c Q_i(s, b, c) = 0$.

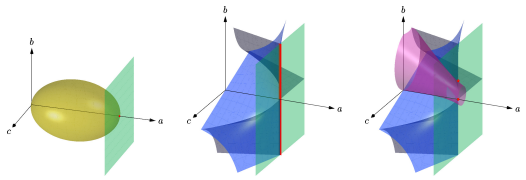

(a) (b) (c)

Fig. 3. Example of events of type A—sweeping plane tangent in a point to a quadrics (a), B—curve of intersection of two quadrics lay in a sweeping plane (b) and (c) a point of intersection of three quadrics lays in a sweeping plane. Sets of points, which induce an event are depicted in red and a sweeping plane is depicted in green

Type B. This type corresponds to the case $s \in K(\rho_{|C_{ij}})$. Such an event corresponds to an a-critical values for which there are solutions to the system $Q_i(s,b,c) = Q_j(s,b,c) = (\nabla Q_i \times \nabla Q_j)_1(s,b,c) = 0$.

Type C. There are values $s \in \rho(P_{ijk})$ above which topology of open connected components in $\mathcal{A}$ changes. An a-critical value is such that there are solutions to the system $Q_i(s,b,c) = Q_j(s,b,c) = Q_k(s,b,c) = 0$. Note that it can happen that an intersection between three quadrics is a curve. This issue can be solved if a curve projects on a point, thanks to the elimination theory and use of resultants or Gröbner basis, by computing univariate polynomial which vanishes on the projection of the curve [6]. For more information about events of the types *A, B* and *C* we refer the reader to [15]. Figure 3 shows examples of events of types A, B and C.

Right now, we are going to discuss the cases of *asymptotic critical values*.

Type A_∞. This type of critical values corresponds to the situation when a plane orthogonal to one of the coordinate axes is tangent to a quadric in a point at infinity (see Figure 4).

Lemma 4. *Let S be a smooth quadric defined by $Q(a,b,c) = 0$. Denoting by $M(a)$ the matrix* $\begin{pmatrix} \frac{\partial^2 Q}{\partial b^2} & \frac{\partial^2 Q}{\partial b \partial c} & \frac{\partial Q}{\partial b}(a,0,0) \\ \frac{\partial^2 Q}{\partial c \partial b} & \frac{\partial^2 Q}{\partial c^2} & \frac{\partial Q}{\partial c}(a,0,0) \end{pmatrix}$ *that depends only on a,*

$$K_\infty(\rho_{|S}) = \{a \mid M(a) \text{ has rank at most } 1\}.$$

Proof. Consider the mapping $f : \mathbb{R}^3 \to \mathbb{R}^2$ such that $(a,b,c) \mapsto (a, Q(a,b,c))$. The definition of K_∞ implies $K_\infty(\rho_{|S}) = K_\infty(f) \cap \mathbb{R} \times \{0\}$. Let $q(a,b,c) = \frac{\max(|\frac{\partial Q}{\partial b}|,|\frac{\partial Q}{\partial c}|)}{\max(|\frac{\partial Q}{\partial a}|,|\frac{\partial Q}{\partial b}|,|\frac{\partial Q}{\partial c}|)}$. Then using [12, Proposition 2.5 and Definition 3.1] with $df = \begin{pmatrix} 1 & 0 & 0 \\ \frac{\partial Q}{\partial a} & \frac{\partial Q}{\partial b} & \frac{\partial Q}{\partial c} \end{pmatrix}$, we have that there exists a sequence $(a_n, b_n, c_n) \in \mathbb{R}^3$ such that $|b_n| + |c_n| \to \infty$ and $a_n \to a$ and $(|b_n| + |c_n|)q(a_n, b_n, c_n) \to 0$. Since $\frac{\partial Q}{\partial a}$, $\frac{\partial Q}{\partial b}$ and $\frac{\partial Q}{\partial c}$ are linear functions, this implies that in the definition of K_∞, the expression $|b_n| + |c_n|$ divided by the denominator of $q(a_n, b_n, c_n)$ is bounded. In particular the numerator of $q(a_n, b_n, c_n)$ converges toward

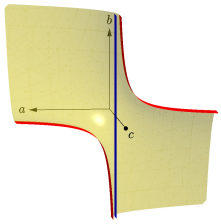

Fig. 4. Example of asymptotic critical value. A line (in blue) is parallel to the b-axis and tangent to a asymptote—red curves laying on the yellow surface—in a point at infinity. For readability only a part of the yellow surface is presented

0. More specifically, $\frac{\partial Q}{\partial b}$ and $\frac{\partial Q}{\partial c}$ converge toward 0. On the other hand, either $|b_n|$ or $|c_n|$ goes toward infinity. Assume without restriction of generality that $|b_n|$ goes toward infinity. In this case, the function $\frac{\partial^2 Q}{\partial c^2}\frac{\partial Q}{\partial b} - \frac{\partial^2 Q}{\partial b \partial c}\frac{\partial Q}{\partial c}$ is a linear function that depends only on b. Then this function converges toward 0 if and only if the coefficient in front of b in this function and its constant coefficient are 0. In particular, if $\frac{\partial^2 Q}{\partial c^2}$ or $\frac{\partial^2 Q}{\partial b \partial c}$ is non-zero, the matrix $M(a)$ has rank 1. If both are 0, then with similar arguments, we can see that $M(a)$ is the null matrix. Thus K_∞ is the set of a such that $M(a)$ has a rank less than or equal 1. □

The algorithm to detect this type of events is as follows. Step 1: we compute $\partial_b Q(a,b,c) = ub + vc + wa + t$ and $\partial_c Q(a,b,c) = u'b + v'c + w'a + t'$, where $u, v, w, t, u', v', w', t' \in \mathbb{Z}$ are coefficients of the corresponding polynomials and $Q \in \mathcal{Q}$. Step 2: let V stands for the cross product of $V_b = (u, v, wa + t)$ and $V_c = (u', v', w'a + t')$, then we solve for a such that all the terms of V are equal 0.

Type B_∞. In this case we are considering the asymptotic critical points of the projection restricted to a curve defined by the intersection of two quadrics $Q_i, Q_j \in \mathcal{Q}$. Using [12, Proposition 4.2], these correspond to the a-coordinate of the sweeping planes that cross the projective closure of the curve at infinity. More formally, we have:

$$K_\infty(\rho_{|C_{ij}}) = \{a \mid \exists (a_n, b_n, c_n) \in C_{ij} \text{ s.t. } |b_n| + |c_n| \to +\infty \text{ and } a_n \to a\}$$

In particular, this set is also the set of values a such that either the projection of C_{ij} on the (a,b)-plane or the projection of C_{ij} on the (a,c)-plane has an asymptote in a.

Using [12, Proposition 4.2], these are the elements of a set of non-properness of the projection map. The properties of this set and algorithms to compute it have been studied notably in [7, 11, 14]. In our case the non-properness set of the projection restricted to C_{ij} is the set of a-coordinates of the sweeping planes that cross at infinity the projective closure of C_{ij}.

To detect such a case we apply the following steps. Step 1: we eliminate the c (resp. b) variable, and we denote the corresponding polynomials as $Pb(a,b)$ (resp. $Pc(a,c)$). Step 2: let $Cb(a)$ and $Cc(a)$ stands for head coefficients—coefficients of leading monomials—of $Pb(a,b)$ and $Pc(a,c)$, respectively. The asymptotic critical value for a pair of quadrics happens for $Cb(a) = 0$ or $Cc(a) = 0$.

4.3 Sorting Critical Values

In this section we focus on the representation of a-critical values as real algebraic numbers—roots of univariate polynomials—and operations such as comparison of them, necessary to sort a-critical values.

Similarly to Mourrain *et al.* [15] we represent a real algebraic number α as a pair: an irreducible univariate polynomial $P \in \mathbb{Z}[a]$ such that $P(\alpha) = 0$ and an open isolating interval $]g, h[, g, h \in \mathbb{Q}$, containing α and such that there is no other root of P in this interval. Note that, the isolation of the roots of an irreducible univariate polynomial can be made using Descartes' rule [27].

Let $\alpha = (P,]g, h[)$ and $\beta = (Q,]i, j[)$ such that $P, Q \in \mathbb{Z}[a]$ and $g, h, i, j \in \mathbb{Q}$, stand for two real algebraic numbers. Then we can conclude if $\alpha = \beta$ while checking that the GCD of P and Q has opposite signs at the bounds of an intersecting interval. On the other hand, to conclude if α is bigger than β or β bigger than α we apply a strategy, which consists of refinement of isolating intervals until their disjointness. When two intervals are disjoint then we can compare their bounds and conclude if α is bigger than β (or β bigger than α) [4]. To refine an isolating interval of real roots, one can use *e.g.*, bisection of intervals, Newton interval method [9], [16, Chapter 5] or quadratic interval refinement method proposed by Abbot [1].

Ability to compare two different algebraic numbers allows us to sort a list of events which can be done with well-known sorting algorithm such as quicksort.

4.4 Sweeping a Set of Quadrics

After sorting the set of a-critical values we are ready to compute sample points of open cells. The sweeping plane moves along the a-axis and stops in between two consecutive a-critical values in a *midpoint*. At such a midpoint we project the set of quadrics onto the sweeping plane by setting their a variable to be equal to the midpoint. This allows us to simplify the problem at a midpoint into the arrangement of conics, which can be solved by applying a strategy similar to the one developed so far, such that we compute and sort a set of b-critical values (or c-critical values) in the arrangement of conics and sweep it by a line. One can also apply the critical points method. Note that we found cylindrical algebraic decomposition practically inefficient for such a problem. Figure 5 shows conics for three a-critical values in an arrangement of two quadrics.

The remaining question is which quadrics we should use at each midpoint to miss no open cell. In our approach we use all the quadrics of $\mathcal{Q}$ for the first midpoint (see Figure 6). Then for any other midpoint we use only the quadrics, related to the lowermost one from the pair, of a-critical values that bound this midpoint. Indeed, doing so we ensure that at the end of our strategy we collect at least one sample point for each full dimensional open cell thanks to Lemma 2, Corollary 3 and Lemma 4.

5 Recovering Translation Parameter Values

The algorithm proposed in the previous section gives us the set $\mathcal{R}$ of sample points $(a, b, c) \in \mathbb{Q}^3$, which correspond to the rotation parameters. In this section we discuss

[4] Our implementation of real algebraic numbers and their comparison can be downloaded from https://github.com/copyme/RigidMotionsMapleTools

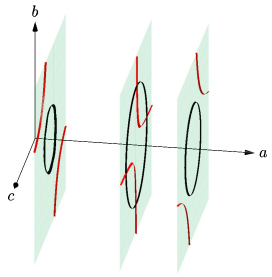

Fig. 5. Visualization of plane sweeping of quadrics. Projection planes at three different midpoints depicted in green. In between the planes we have a-critical values – a values in which topology of an arrangement changes. Conics obtain from quadrics in red and black

how to obtain sample points (t_1, t_2, t_3) of the translation part for each $(a, b, c) \in \mathcal{R}$ and how to generate different images of an image patch under rigid motions.

Let us first note that Equation (3) under the assumption of $\mathbf{t} \in \left(-\frac{1}{2}, \frac{1}{2}\right)^3$ defines the set of planes in the range $\boldsymbol{\mathcal{P}} = \left(-\frac{1}{2}, \frac{1}{2}\right)^3$ for each $(a, b, c) \in \mathcal{R}$, by setting $\mathbf{v} \in \mathcal{N}$ and $\mathbf{k} \in H(\mathcal{N})^3$. These planes divide $\boldsymbol{\mathcal{P}}$ into cuboidal regions. Figure 7 illustrates an example of such critical planes in $\boldsymbol{\mathcal{P}}$.

To obtain different images of an image patch $\mathcal{N}$ rotated by a given $a, b, c \in \mathbb{Q}$, under translations $(t_1, t_2, t_3) \in \boldsymbol{\mathcal{P}}$, we compute the arrangement of planes in $\boldsymbol{\mathcal{P}}$ which involves sorting of critical planes and finding a midpoint of each cuboidal region bounded by them.

Remark 1. Note that we can have several sample points (a, b, c) inducing the topologically equivalent arrangement of planes (the order of planes is identical). Therefore, to avoid unnecessary calculations we can define a hash function $\mathcal{H}$ which returns a different signature for each sample point (a, b, c) which induce a different order of the critical planes.

To define a hash function $\mathcal{H}$, let $\mathcal{I}$ stands for a collection of indexes of critical planes. Then we define the hash function that returns the sorted indices of $\mathcal{I}$ with respect to the order of critical planes.

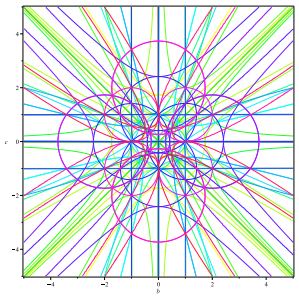

Fig. 6. The first projection of 81 quadrics obtain for the image patch $\mathcal{N} = \{(1, 0, 0), (0, 1, 0), (0, 0, 1), (0, 0, 0), (-1, 0, 0), (0, -1, 0), (0, 0, -1)\}$

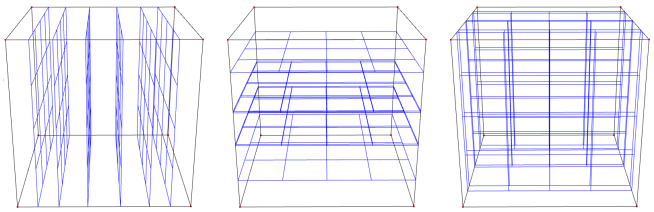

(a) (b) (c)

Fig. 7. Visualization of the critical planes for $\mathcal{N} = \{(1,0,0),(0,1,0),(0,0,1),(0,0,0),(-1,0,0),(0,-1,0),(0,0,-1)\}$ and some (a,b,c). For the sake of visibility three types of orthogonal critical planes are presented separately

6 A Case Study

In this section we would like to address some issues of the proposed algorithm while considering a particular image patch $\mathcal{N}$. Hereafter, we consider $\mathcal{N} = \{(1,0,0),(0,1,0),(0,0,1),(0,0,0),(-1,0,0),(0,-1,0),(0,0,-1)\}$.

6.1 Combinatorial Issue

The number of quadrics obtain directly from Equation (8) for $\mathcal{N}$ is 441. In this section we will show that this number is reduced to 81 by discarding those which are always strictly positive (resp. negative) and ones which are redundant. Note that similar studies remain valid for different image patches.

Let us consider vectors $\mathbf{u}_1 = (1,0,0)$ (resp. $\mathbf{u}_2 = (0,1,0)$, $\mathbf{u}_3 = (0,0,1)$) and $\mathbf{h} = \left(\frac{1}{2},\frac{1}{2},\frac{1}{2}\right)$. Then we obtain the following inequality from (6)

$$\mathbf{u}_i \cdot (\mathbf{k}' - \mathbf{h} - \mathbf{R}\mathbf{v}') < \mathbf{u}_i \cdot (\mathbf{k} + \mathbf{h} - \mathbf{R}\mathbf{v}) \tag{9}$$

for $i = 1,2,3$ where $\mathbf{v},\mathbf{v}' \in \mathcal{N}, \mathbf{k},\mathbf{k}' \in H(\mathcal{N})^3$. This induces

$$k_i - k_i' + 1 - \mathbf{u}_i \cdot \mathbf{R}(\mathbf{v} - \mathbf{v}') > 0, \tag{10}$$

where we know that $K = k_i - k_i' + 1 \in \mathbb{Z} \cap [-1,3]$. We then consider the following different cases of $\bar{V} = \|\mathbf{v} - \mathbf{v}'\|$:

1. when $\bar{V} = 0$, then there is no $K \in \mathbb{Z} \cap [-1,3]$ satisfying (10),
2. when $\bar{V} = 1$, then there are 6 different pairs of $(\mathbf{v},\mathbf{v}')$ and we obtain $K \in \{0\}$,
3. when $\bar{V} = 2$, then there are 6 different pairs of $(\mathbf{v},\mathbf{v}')$ and we obtain $K \in \{-1,0,1\}$,
4. when $\bar{V} = \sqrt{2}$, then there are 12 different pairs of $(\mathbf{v},\mathbf{v}')$ and we obtain $K \in \{-1,0,1\}$.

Therefore, the number of valid quadrics $Q[\mathbf{v},\mathbf{v}',k_i,k_i']$ for each case is 0 (case 1), 6 (case 2), 18 (case 3) and 36 (case 4). Note that case 2 is included in case 3 up to a constant, as that we can ignore the 6 quadrics. This finally gives us $\frac{18+36}{2} = 27$ quadrics per direction and thus 81 in total.

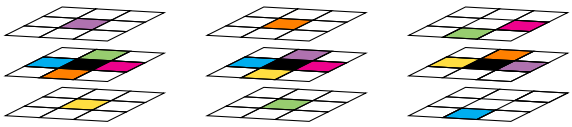

Fig. 8. Visualization of (a) the image patch $\mathcal{N} = \{(1,0,0),(0,1,0),(0,0,1),(0,0,0),(-1,0,0),(0,-1,0),(0,0,-1)\}$ and its images under digitized rigid motions: the rotation given by $a = \frac{330688038827}{274877906944}, b = 7, c = 9$ followed by the translation (b) $\mathbf{t} = \mathbf{0}$ and (c) $\mathbf{t} = (-\frac{35}{100}, \frac{28}{100}, \frac{4}{10})$. For a sake of simplification, $\mathcal{N}$ is presented layer-by-layer. Each point of $\mathcal{N}$ is represented by a colored square with **c** in black

6.2 Implantation and Experiments

We have implemented the proposed algorithm in Maple 2015 and our code can be downloaded from https://github.com/copyme/RigidMotionsMapleTools. In our implementation we have tried to obtain a good performance. Since the computation of critical values and sample points are not difficult to parallelize, we implemented this part of the algorithm in the Maple Grid framework and we performed tests on a machine equipped with two processors Intel(R) Xeon(R) E5-2680 v2; clocked at 2.8 GHz, with installed 251.717 GiB of memory. After the uncoupling, we obtained 81 quadrics, as predicted. Computation of sample points in such an arrangement took for 20, 15, 10, 5 computational nodes around 16, 19, 22 and 33 minutes, respectively. Notice that computing and sorting of critical values took around 2 minutes for 20–10 nodes and around 3 minutes for 5 nodes. Note that, sorting of critical values was performed on one node. Moreover, computations in such setting need around 21 GiB of memory. Presented real time and memory usage were obtained thanks to the Maple function `Usage` from the package `CodeTools`. In our implementation we used for each arrangement of conics the critical point method implemented in RAGlib which returns rational sample points [28]. Note that the average of the number of conics per midpoint is around 11.

Finally, for all the obtained each sample point (a,b,c) we recovered the different images of the image patch under digitized rigid motions which took again around 18, 22, 28 and 42 minutes for 20, 15, 10 and 5 nodes respectively[5]. Note that the memory usage did not exceed few mebibytes. The computation of different images of the image patch $\mathcal{N}$ consists of calculating for each sample point (a,b,c) an arrangement of planes (see Figure 7). In such an arrangement each sample point (t_1,t_2,t_3) of full dimensional cell bounded by planes represents the translation part of rigid motions. Using this information we generate an image of the image patch $\mathcal{N}$, by appling to it a digitized rigid motion given by the value of (a,b,c,t_1,t_2,t_3). Note that for different sample points (a,b,c) that belong to the same full dimensional component we observe that planes presented in Figure 7 move but they do not change their order. Figure 8 shows some images of an image patch for fixed (a,b,c) values and different (t_1,t_2,t_3) values.

[5] Note that this time is affected by a time needed to read a list of sample points (a,b,c) from a hard drive before the main computations.

7 Conclusions

In this article, we proposed a method to decompose the 6D parameter space of digitized rigid motions for a given 3D image patch. We first uncouple the six parameters of 3D rigid motions to end up with two systems in three variables, and start by studying an arrangement of quadrics in $\mathbb{R}^3$.

Our approach to compute an arrangement of quadrics in 3D is similar to the one proposed by Mourrain *et al.* [15] where the main differences are; we do not use generic directions: we handle asymptotic cases and give new criteria to compute critical values in polynomials of degree two; we compute and store at least one sample point for each full dimensional open cell where Mourrain *et al.* [15] compute full adjacency information for all cells in an arrangement; moreover, we precompute all critical values *a priori* while in the former approach only one type of critical values needs to be computed before the main algorithm. Those sample points are then used to decompose the other three-dimensional parameter space. We also provided our implementation together with a numerical experiment for some small image patch.

As a part of our future work we would like to use the presented method in a study of topological alteration of $\mathbb{Z}^3$ under 3D digitized rigid motions.

Acknowledgments. This work received funding from the project Singcast (ANR–13–JS02–0006).

References

1. Abbott, J.: Quadratic Interval Refinement for Real Roots. Communications in Computer Algebra 48(1/187), 3–12 (2014)
2. Amir, A., Kapah, O., Tsur, D.: Faster two-dimensional pattern matching with rotations. Theoretical Computer Science 368(3), 196–204 (2006)
3. Basu, S., Pollack, R., Roy, M.F.: Algorithms in real algebraic geometry. Springer Berlin Heidelberg (2005)
4. Cayley, A., Forsyth, A.: The Collected Mathematical Papers of Arthur Cayley, vol. 1. The University Press (1898)
5. Collins, G.: Quantifier elimination for real closed fields by cylindrical algebraic decomposition. In: Automata Theory and Formal Languages. LNCS, vol. 33, pp. 134–183. Springer Vienna (1975)
6. Cox, D., Little, J., O'Shea, D.: Ideals, Varieties and Algorithms. An Introduction to Computational Algebraic Geometry and Commutative Algebra. Springerr-Verlag New York (1996)
7. El Din, M.S., Schost, E.: Properness Defects of Projections and Computation of at Least One Point in Each Connected Component of a Real Algebraic Set. Discrete & Computational Geometry 32(3), 417 (2004)
8. Halperin, D.: Arrangements. In: Goodman, J.E., O'Rourke, J. (eds.) Handbook of Discrete and Computational Geometry, 2nd Ed., pp. 529–562. Chapman and Hall/CRC (2004)
9. Hansen, E.: Global optimization using interval analysis – the multi-dimensional case. Numerische Mathematik 34(3), 247–270 (1980)
10. Hundt, C., Liskiewicz, M.: On the Complexity of Affine Image Matching. In: STACS. Lecture Notes in Computer Science, vol. 4393, pp. 284–295. Springer Berlin Heidelberg (2007)
11. Jelonek, Z.: Topological characterization of finite mappings. Bull. Polish Acad. Sci. Math 49(3), 279–283 (2001)
12. Jelonek, Z., Kurdyka, K.: Quantitative generalized Bertini-Sard theorem for smooth affine varieties. Discrete & Computational Geometry 34(4), 659–678 (2005)

13. Kurdyka, K., Orro, P., Simon, S., et al.: Semialgebraic Sard theorem for generalized critical values. Journal of differential geometry 56(1), 67–92 (2000)
14. Moroz, G.: Properness defects of projection and minimal discriminant variety. Journal of Symbolic Computation 46(10), 1139–1157 (2011)
15. Mourrain, B., Tecourt, J.P., Teillaud, M.: On the computation of an arrangement of quadrics in 3D. Computational Geometry 30(2), 145–164 (2005)
16. Neumaier, A.: Interval Methods for Systems of Equations. Encyclopedia of Mathematics and its Applications, Cambridge University Press Cambridge (1991)
17. Ngo, P., Kenmochi, Y., Passat, N., Talbot, H.: Combinatorial structure of rigid transformations in 2D digital images. Computer Vision and Image Understanding 117(4), 393–408 (2013)
18. Ngo, P., Kenmochi, Y., Passat, N., Talbot, H.: Topology-preserving conditions for 2D digital images under rigid transformations. Journal of Mathematical Imaging and Vision 49(2), 418–433 (2014)
19. Ngo, P., Passat, N., Kenmochi, Y., Talbot, H.: Topology-preserving rigid transformation of 2D digital images. IEEE Transactions on Image Processing 23(2), 885–897 (2014)
20. Nouvel, B., Rémila, E.: On colorations induced by discrete rotations. In: DGCI, Proceedings. Lecture Notes in Computer Science, vol. 2886, pp. 174–183. Springer (2003)
21. Nouvel, B., Rémila, E.: Configurations induced by discrete rotations: Periodicity and quasi-periodicity properties. Discrete Applied Mathematics 147(2–3), 325–343 (2005)
22. Pluta, K., Kenmochi, Y., Passat, N., Talbot, H., Romon, P.: Topological alterations of 3D digital images under rigid transformations. Research report, Université Paris-Est, Laboratoire d'Informatique Gaspard-Monge UMR 8049 (2014), https://hal.archives-ouvertes.fr/hal-01333586
23. Pluta, K., Romon, P., Kenmochi, Y., Passat, N.: Bijective rigid motions of the 2D Cartesian grid. In: DGCI. pp. 359–371. Lecture Notes in Computer Science, Springer (2016)
24. Pluta, K., Romon, P., Kenmochi, Y., Passat, N.: Bijectivity Certification of 3D Digitized Rotations. In: CTIC. Lecture Notes in Computer Science, vol. 9667, pp. 30–41. Springer International Publishing Switzerland (2016)
25. Rabier, P.J.: Ehresmann fibrations and Palais-Smale conditions for morphisms of Finsler manifolds. Annals of Mathematics pp. 647–691 (1997)
26. Renegar, J.: On the computational complexity and geometry of the first-order theory of the reals. Part I: Introduction. Preliminaries. The geometry of semi-algebraic sets. The decision problem for the existential theory of the reals. Journal of symbolic computation 13(3), 255–299 (1992)
27. Rouillier, F., Zimmermann, P.: Efficient isolation of polynomial's real roots . Journal of Computational and Applied Mathematics 162(1), 33–50 (2004)
28. Safey El Din, M.: Testing sign conditions on a multivariate polynomial and applications. Mathematics in Computer Science 1(1), 177–207 (2007)
29. Singla, P., Junkins, J.L.: Multi-resolution methods for modeling and control of dynamical systems. CRC Press Boca Raton (2008)
30. Thibault, Y.: Rotations in 2D and 3D discrete spaces. Ph.D. thesis, Université Paris-Est (2010)
31. Thibault, Y., Sugimoto, A., Kenmochi, Y.: 3D discrete rotations using hinge angles. Theoretical Computer Science 412(15), 1378–1391 (2011)
32. Yilmaz, A., Javed, O., Shah, M.: Object tracking: A survey. Acm computing surveys (CSUR) 38(4), 13 (2006)
33. Zitova, B., Flusser, J.: Image registration methods: a survey. Image and vision computing 21(11), 977–1000 (2003)